

Chemical Science

Accepted Manuscript

This article can be cited before page numbers have been issued, to do this please use: S. Zang, J. Ke, H. Zheng, Q. Liu, Y. Liu, C. Yao, B. Wang, M. Lan and X. Song, *Chem. Sci.*, 2026, DOI: 10.1039/D6SC01655C.



This is an Accepted Manuscript, which has been through the Royal Society of Chemistry peer review process and has been accepted for publication.

Accepted Manuscripts are published online shortly after acceptance, before technical editing, formatting and proof reading. Using this free service, authors can make their results available to the community, in citable form, before we publish the edited article. We will replace this Accepted Manuscript with the edited and formatted Advance Article as soon as it is available.

You can find more information about Accepted Manuscripts in the [Information for Authors](#).

Please note that technical editing may introduce minor changes to the text and/or graphics, which may alter content. The journal's standard [Terms & Conditions](#) and the [Ethical guidelines](#) still apply. In no event shall the Royal Society of Chemistry be held responsible for any errors or omissions in this Accepted Manuscript or any consequences arising from the use of any information it contains.

ARTICLE

A chemo-selective deprotection–cyclization strategy enables fluorescent imaging of hydroxylamine and reveals its pathologic role in Parkinson's disease

Shunping Zang,^{a†} Jia Ke,^{b†} Hanbing Zheng,^a Qing Liu,^a Liu Yang,^a Chaoyi Yao,^{*a} Benhua Wang,^{*a} Minhuan Lan,^a and Xiangzhi Song^{*a}

Received 00th January 20xx,
Accepted 00th January 20xx

DOI: 10.1039/x0xx00000x

Hydroxylamine (HA), a reactive nitrogen species generated by neuronal nitric oxide synthase (nNOS), has been largely overlooked in neurodegenerative disorders. Herein, we report the first identification of HA overexpression in Parkinson's disease (PD) and elucidate its pathological role using chemo-selective fluorescence imaging combined with proteomic analysis. A general HA-responsive probe platform was developed by introducing a 1-(4,4-dimethyl-2,6-dioxacyclohexylidene)ethyl (Dde) unit as a highly specific HA-recognition motif. Among the resulting probes, **DCI-HA-2** exhibited remarkable sensitivity, fast response, and excellent selectivity toward HA. Using **DCI-HA-2**, elevated HA levels were visualized in PD cells, PD model mice, and brain tissues for the first time. Mechanistically, nNOS-derived HA suppresses cystathionine β -synthase (CBS) expression, leading to impaired hydrogen sulfide (H₂S) biosynthesis, and simultaneously induces adenosine-5'-triphosphate (ATP) depletion, thereby disrupting adenosine 5'-monophosphate-activated protein kinase (AMPK) signaling in PD pathology. This work identifies HA as a previously unrecognized pathological regulator in PD, and establishes a powerful chemical strategy for probing HA-associated pathological processes in complex biological systems.

Introduction

Accumulating evidence suggests that reactive nitrogen species (RNS) derived from neuronal nitric oxide synthase (nNOS) have been closely implicated in Parkinson's disease (PD) pathogenesis, a progressive neurodegenerative disorder without effective therapeutic intervention.^{1–6} While canonical RNS such as nitric oxide (NO), nitroxyl (HNO), and peroxyxynitrite (ONOO[•]) have been extensively investigated in PD, comparatively little attention has been devoted to hydroxylamine (HA), an important downstream metabolite intimately linked to nNOS-associated nitrogen redox pathways.^{7–9} Emerging studies reveal that elevated level of HA can inhibit cystathionine β -synthase (CBS) and succinate oxidase activity.^{10–12} HA has also been reported to possess a neurological relaxation effect.¹³ Despite these observations, the exact level of HA in PD and how it may contribute to PD progression remain unknown. The limited exploration of HA in PD is largely due to the lack of reliable methods for HA selective detection in complex pathological conditions.

Fluorescence imaging has emerged as a powerful tool for biomarker detection and therapeutic evaluation in neurological

diseases owing to its high sensitivity, selectivity, noninvasiveness, and *in situ* imaging capability.^{14–19} However, selective HA recognition remains a challenge, as HA is a highly reactive nitrogen-containing nucleophile that coexists with numerous endogenous interferents. To date, only a few fluorescent probes for HA detection have been reported (Table S1), and most rely on the nucleophilic addition or condensation with electrophilic motifs.^{20–25} Although such designs are synthetically accessible, they often suffer from cross-reactivity with endogenous nucleophiles, including hydrogen sulfide (H₂S), thiols, sulfur dioxide derivatives, and ONOO[•].^{26–29} For example, probe **1** responds to both HA and H₂S, while the HA probe **RhChr** displays cross-reactivity toward ONOO[•] (Table S1).^{30,31} Therefore, the development of a fundamentally distinct recognition mechanism that enables highly selective detection of HA for elucidating its fluctuation and mechanistic examination in PD is highly desirable.

Inspired by classic deprotection chemistry, we turn our attention to the 1-(4,4-dimethyl-2,6-dioxacyclohexylidene)ethyl (Dde) group, an amine-protecting moiety that undergoes selectively cleavage by HA under mild conditions.^{32,33} Based on this unique reactivity, we envisioned that the Dde motif could be repurposed as a HA-specific chemical trigger in living systems. Such a strategy exploits the intrinsic and preferential reactivity of HA toward Dde deprotection, which averts the interfere from biological nucleophilic species.³⁴ Additionally, when coupled to fluorophores bearing masked electron-donating groups, HA-mediated Dde cleavage can initiate an intramolecular cyclization cascade, resulting in fluorophore release and signal

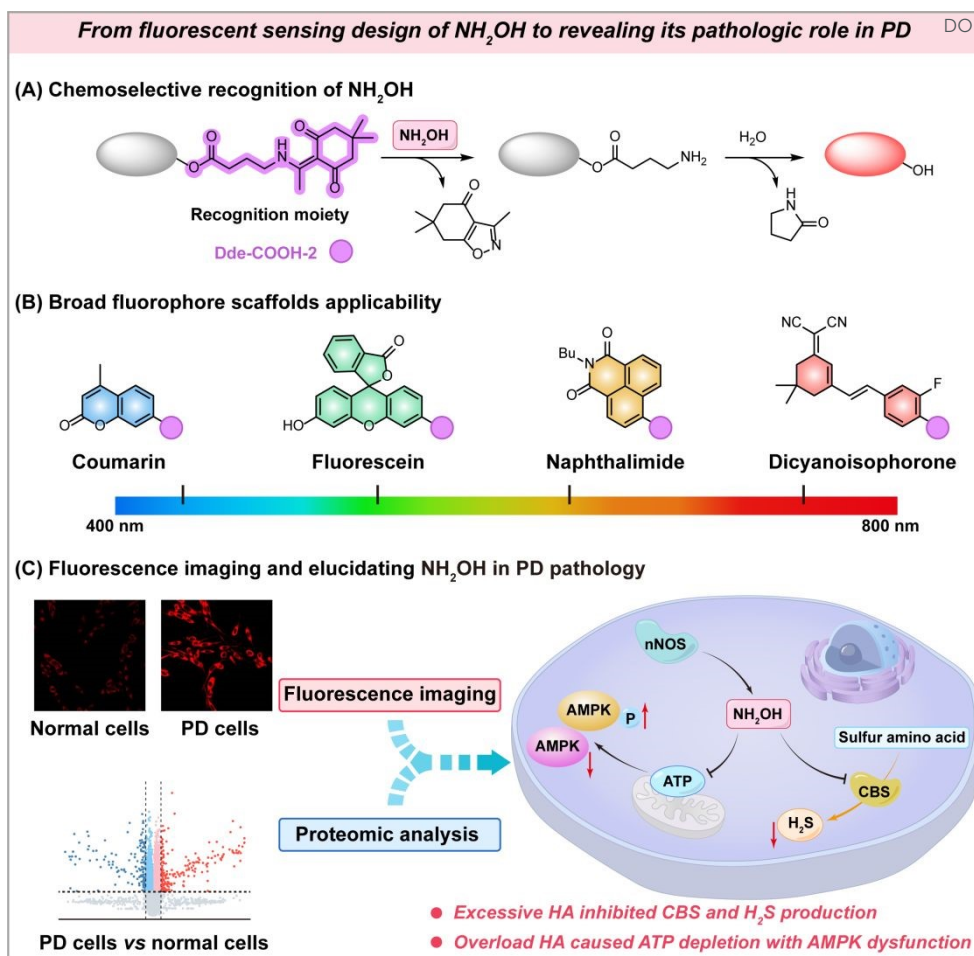
^a College of Chemistry and Chemical Engineering, Central South University, Changsha, Hunan 410083, P.R. China. E-mails: chaoyiyao@csu.edu.cn; benhuawang@csu.edu.cn; xzsong@csu.edu.cn.

^b Liangzhu Laboratory, Zhejiang University Medical Center, Hangzhou, Zhejiang 311121, P.R. China.

† These authors contributed to this work equally.

Electronic supplementary information (ESI) available. See DOI: 10.1039/x0xx00000x





Scheme 1 Design strategy for HA-activated fluorescent probes and schematic illustration of elucidating its pathologic role in PD.

amplification. This deprotection–cyclization mechanism offers a conceptually generalizable platform for HA-selective probe development.

Herein, we report a chemo-selective “deprotection–cyclization” strategy for HA recognition based on Dde chemistry and establish a general fluorescent probe platform applicable to multiple fluorophore scaffolds (Scheme 1). The optimized probe, **DCI-HA-2**, enabled rapid, sensitive, and exceptional selective detection of HA in cells and *in vivo*. Using this probe, we achieved, for the first time, the real-time imaging of elevated HA levels in PD focal cells and PD model mice. Importantly, by integrating fluorescence imaging with proteomic analysis, we uncovered a previously unrecognized pathogenic pathway in which nNOS-derived HA suppresses the expression of CBS, leading to reduced cellular H_2S production, and concurrently induces ATP depletion with subsequent downregulation of the AMPK signaling pathway during PD progression. Overall, this study not only provides a chemo-selective strategy for HA detection, but also unveils HA-associated pathogenic mechanisms in PD, thereby opening new avenues for improved pathological research and targeted therapeutic intervention.

Results and discussion

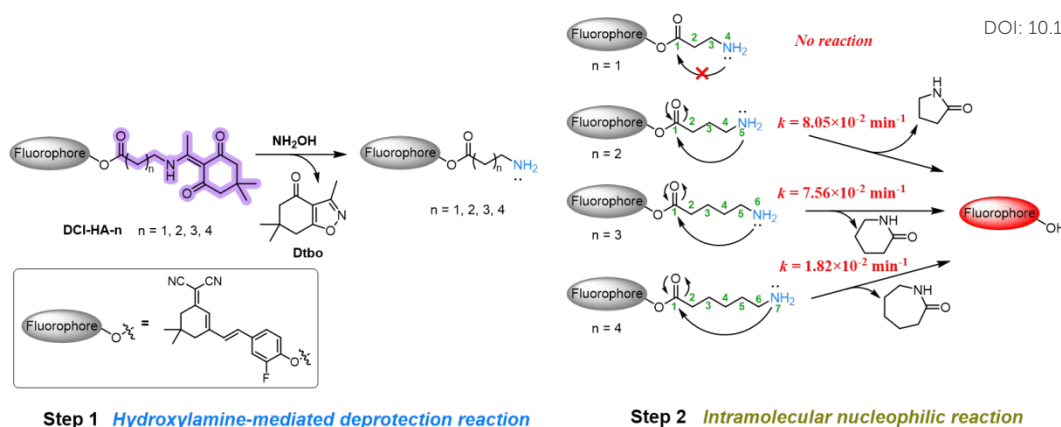
Molecular design and synthesis of probes

To enable deeper brain imaging in PD models, the dicyanoisophorone (DCI) fluorophore was first selected as the fluorophore due to its favorable blood-brain barrier (BBB) permeability and red-emission optical properties.^{35, 36} To further optimize probe's kinetics and sensitivity, a series of Dde-protected probes (**DCI-HA-*n***, *n* = 1–4) with different linker lengths between the free amine and the carbonyl group were synthesized (Schemes S1 and S2) for investigations. Upon exposure to HA, the Dde-protected amine is first deprotected to generate a free primary amine (Step 1), which subsequently initiates intramolecular nucleophilic cyclization and releases the active fluorophore (Step 2), thereby restoring fluorescence (Scheme 2). All compounds were fully characterized by HRMS, ^1H NMR and ^{13}C NMR spectroscopy (Figs. S29–S68).

Photophysical properties and response mechanism of probes towards HA

The photophysical properties and response kinetics of probes **DCI-HA-*n*** towards HA were first investigated in PBS buffer (10.0 mM, pH = 7.40, containing 1% DMSO). As seen in Figs. 1A–1D, in the absence of HA, all probes displayed a characteristic absorption peak around 395 nm. Upon addition of HA (10.0 μM), **DCI-HA-2**, **DCI-HA-3**, and **DCI-HA-4** displayed a pronounced red shift to 470 nm, indicative of Dde deprotection and subsequent structural transformation, whereas **DCI-HA-1**





Scheme 2 Investigation and proposed process of HA recognition in probes with various length cleavable linkers.

exhibited almost no spectral change, hinting ineffective cyclization due to its short linker. Correspondingly, **DCI-HA-2**, **DCI-HA-3** and **DCI-HA-4** showed obvious fluorescence emission at 675 nm, with 31.0-fold, 27.7-fold and 19.3-fold fluorescence enhancement, respectively. In addition, the response rate of these probes was strongly dependent on the length of the cleavable linker, following the order: **DCI-HA-2** (30.0 min) > **DCI-HA-3** (45.0 min) > **DCI-HA-4** (120 min) (Fig. S1).

To verify the proposed sensing mechanism, HRMS analysis was performed. As illustrated in Figs. S2–S5, the mass peaks at $[M+H]^+ = 180.1025$ and $[M + Na]^+ = 202.0844$ correspond to the expected deprotected product, **Dtbo** (Scheme 2, $M = 179.0946$), confirming HA-mediated cleavage of the Dde group. For the mixture of **DCI-HA-1** with HA, a peak at $m/z = 380.1768$ was observed, corresponding to the expected intermediate **DCI-HA-1-NH₂**, consistent with its inability to undergo intramolecular cyclization (Fig. S2). In contrast, cyclic intermediates and the released fluorophore **DCI-OH** were observed in the mixtures of **DCI-HA-2**, **DCI-HA-3**, and **DCI-HA-4** with HA, respectively, validating the proposed cyclization–release mechanism (Figs. S3–S5). The variation in response times among **DCI-HA-2**, **DCI-**

HA-3, and **DCI-HA-4** is attributed to inker-length-dependent intramolecular reaction rates.^{37–39} Among these probes, **DCI-HA-2** exhibited the most favorable response characteristics and was selected for further studies.

Subsequently, we systematically investigated the spectral response of **DCI-HA-2** towards HA. As shown in Fig. 1E, the fluorescence intensity at 675 nm gradually increased after adding HA (0–50.0 μ M). A good linear relationship between fluorescence intensity and HA concentration was observed in the range of 0–20.0 μ M, and the limit of detection (LOD) was calculated to be 21.6 nM (Fig. 1F). To validate the specificity, the fluorescence responses of **DCI-HA-2** toward various biologically relevant species were examined. As shown in Fig. 1G, common metal ions (Fe^{3+} , Fe^{2+} , Zn^{2+} , Mg^{2+} , Cu^{2+} and Ca^{2+}), reactive sulfur species (HSO_3^- , SO_3^{2-} , $S_2O_3^{2-}$ and S_2^-), reactive oxygen species (H_2O_2 , $\cdot OH$, $O_2^{\cdot -}$ and $HOCl$), reactive nitrogen species (NO_2^- , NO_3^- , $ONOO^-$, HNO and NO), biothiols (Cys, Hcy, GSH, GSSG), and L-arginine induced negligible fluorescence changes, whereas HA triggered a pronounced fluorescence enhancement. Moreover, the fluorescence response of **DCI-HA-2** toward HA was not affected in the presence of these potential interferents (Fig. S6).

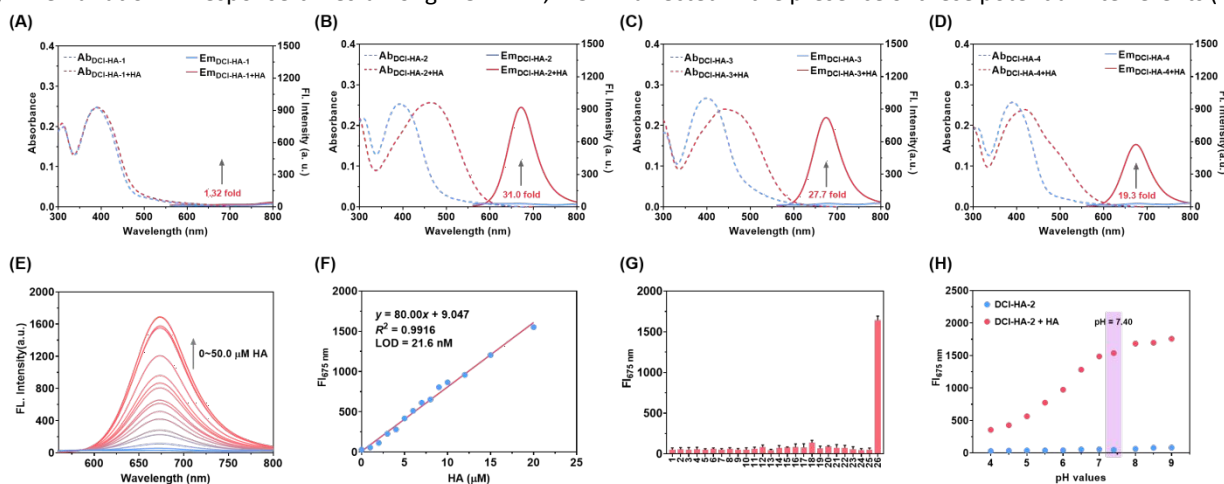


Fig. 1 Absorption (dotted lines) and fluorescence (solid lines) spectra of **DCI-HA-n** (10.0 μ M) before (blue lines) and after (red lines) addition of HA (10.0 μ M) for 30.0 min. (A) **DCI-HA-1**, (B) **DCI-HA-2**, (C) **DCI-HA-3** and (D) **DCI-HA-4**. (E) Fluorescence spectra of **DCI-HA-2** (10.0 μ M) with increasing HA concentrations (0–50.0 μ M). (F) Linear relationship between fluorescence intensity at 675 nm and HA concentration (0–20.0 μ M). (G) Fluorescence intensity at 675 nm of **DCI-HA-2** (10.0 μ M) towards various bioactive substances (1~26: Blank, Fe^{3+} , Fe^{2+} , Zn^{2+} , Mg^{2+} , Cu^{2+} , Ca^{2+} , HSO_3^- , SO_3^{2-} , $S_2O_3^{2-}$, S_2^- , H_2O_2 , $\cdot OH$, $O_2^{\cdot -}$, $HOCl$, NO_2^- , NO_3^- , $ONOO^-$, HNO , NO , Cys, Hcy, GSH, GSSG, L-arginine and HA; other species at 20.0 μ M, GSH at 1.0 mM). (H) Fluorescence intensity at 675 nm of **DCI-HA-2** (10.0 μ M) towards HA (20.0 μ M) in various pH values buffer. Data are expressed as mean \pm SD, $n = 3$. $\lambda_{ex} = 480$ nm. Test media: PBS buffer (pH = 7.40, 10 mM) with 1% DMSO.



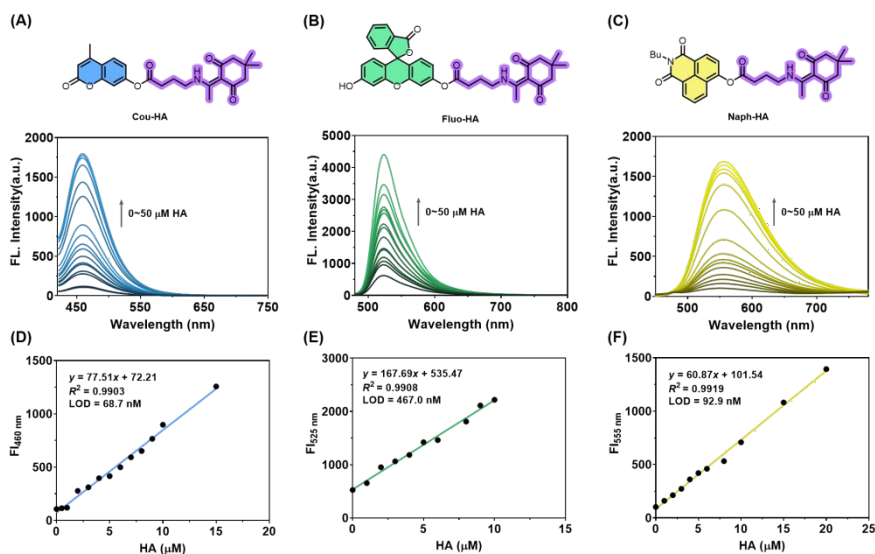


Fig. 2 Molecular structures of probes and their concentration-dependent fluorescence responses toward HA (0–50.0 μM): (A) **Cou-HA**, (B) **Fluo-HA**, and (C) **Naph-HA**, respectively. Probe concentration: 10.0 μM . Linear relationship between fluorescence intensity of (D) **Cou-HA** at 460 nm, (E) **Fluo-HA** at 525 nm, and (F) **Naph-HA** at 555 nm to HA concentration. $\lambda_{\text{ex}} = 405$ nm for **Cou-HA**, $\lambda_{\text{ex}} = 450$ nm for **Fluo-HA**, and $\lambda_{\text{ex}} = 420$ nm for **Naph-HA**. Test media: PBS buffer (pH = 7.40, 10 mM) with 1% DMSO.

Despite N_2H_4 is the other reagent that can deprotect Dde (Fig. S7). However, N_2H_4 is unlikely to interfere the detection of HA by using **DCI-HA-2** because N_2H_4 is not present in most living systems. The performance of **DCI-HA-2** under physiological environment was further investigated. As seen in Fig. 1H, **DCI-HA-2** remained good stability over a broad pH range, and a significant fluorescence increase was observed upon HA addition in the pH range of 7.00–9.00, indicating its suitability for HA detection in living systems. Therefore, these results verify that **DCI-HA-2** enables highly sensitive and selective detection of HA under biological conditions, highlighting its potential for real-time imaging of HA dynamics in living cells and brain.

To further verify the universality of the design strategy, coumarin, fluorescein, and naphthalimide fluorophores were employed to develop HA-activated probes, namely **Cou-HA**, **Fluo-HA**, and **Naph-HA** (Fig. 2). Their synthetic routes are shown in Scheme S3 and their fluorescence behaviors of these probes toward HA were investigated. As seen in Figs. 2A–2C, all three probes presented marked fluorescence enhancements at 460 nm, 525 nm and 555 nm, respectively, upon the addition of HA, accompanied by corresponding absorption changes (Fig. S8). Moreover, each probe exhibited a good linear fluorescence response toward HA: 0–15.0 μM with $R^2 = 0.9903$ for **Cou-HA** (Fig. 2D), 0–10.0 μM with $R^2 = 0.9908$ for **Fluo-HA** (Fig. 2E), and 0–20.0 μM with $R^2 = 0.9919$ for **Naph-HA** (Fig. 2F). The LOD values were determined as 68.7, 467.0, and 92.9 nM, respectively. In addition, all three probes exhibited high selectivity (Fig. S9), anti-interference performance (Fig. S10) and good photostability (Fig. S11). Overall, these results confirm that the Dde-COOH-2 moiety serves as a robust and versatile chemoselective handle for constructing HA-responsive probes.

Fluorescence imaging of exogenous and endogenous cellular HA

Low cytotoxicity and good biocompatibility are crucial for fluorescent probes used in cellular and brain imaging. To evaluate these, the cytotoxicity of **DCI-HA-2** was examined by MTT assays. As seen in Fig. S12, PC-12 cells treated with **DCI-HA-**

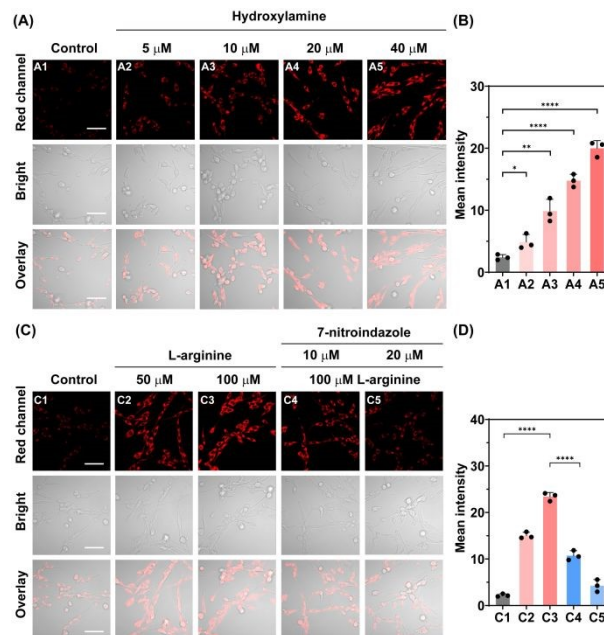


Fig. 3 Fluorescence imaging of exogenous and endogenous HA in PC-12 cells. (A) Cells were incubated with various concentrations of HA (0, 5.0, 10.0, 20.0 and 40.0 μM) for 1 h and then stained with **DCI-HA-2** (10.0 μM) for 30 min. (B) Quantification of mean fluorescence intensity corresponding to panel (A). (C) PC-12 cells subjected to different pre-treatments before incubation with **DCI-HA-2** (10.0 μM) for 30 min. (C1–C3) Cells incubated with L-arginine (0, 50.0 and 100 μM) for 4 h. (C4 and C5) Cells pre-incubated with 7-nitroindazole (10.0 and 20.0 μM) for 8 h, followed by L-arginine (100 μM) for 4 h. (D) Quantification of mean fluorescence intensity corresponding to panel (C). $\lambda_{\text{ex}} = 488$ nm, $\lambda_{\text{em}} = 620$ –720 nm. Scale bar = 50.0 μm . Error bars represent SD, $n = 3$. **** $p < 0.0001$, ** $p < 0.01$, * $p < 0.05$.



2 (10.0 μM) for 24 h exhibited a viability of 93.6%. Moreover, hematoxylin-eosin (H&E) staining indicated no discernible histological or morphological differences between the sham group and the probe-treated group (Fig. S13), confirming the biocompatibility of **DCI-HA-2**. We firstly investigated the ability of **DCI-HA-2** to visualize the fluctuations of exogenous HA in living cells. As depicted in Fig. 3A, PC-12 cells incubated with **DCI-HA-2** alone exhibited faint red fluorescence, indicating a low intrinsic level of intracellular HA under normal conditions. In contrast, when cells were pre-incubated with increasing concentrations of HA (0.0, 5.0, 10.0, 20.0 and 40.0 μM) prior to **DCI-HA-2** staining, the red fluorescence intensity increased progressively (Fig. 3B), implying that **DCI-HA-2** is capable of sensitively monitoring exogenous HA levels in living cells. Next, we evaluated the capability of **DCI-HA-2** to track endogenous HA production.

L-arginine was used as a precursor for endogenous HA generation via nNOS-catalyzed reaction,⁴⁰ while 7-nitroindazole, a selective inhibitor of nNOS, was used to suppress HA production.⁴¹ As shown in Fig. 3C, incubation of PC-12 cells with L-arginine (50.0 and 100.0 μM) led to a marked enhancement of red fluorescence, corresponding to 6.81- and 9.98-fold increase, respectively, confirming the endogenous nNOS-mediated generation of intracellular HA. However, pre-treatment of cells with 7-nitroindazole (10.0 and 20.0 μM), followed by stimulation with L-arginine (100 μM), led to a pronounced attenuation of fluorescence signals to 0.18- and 0.12-fold, respectively (Fig. 3D), suggesting effective inhibition of nNOS-dependent HA generation. These results indicate that **DCI-HA-2** can sensitively monitor endogenous HA fluctuations in living PC-12 cells under pharmacological modulation.

Fluorescence imaging of HA change in PD model cells

To further evaluate the HA dynamics under PD pathological

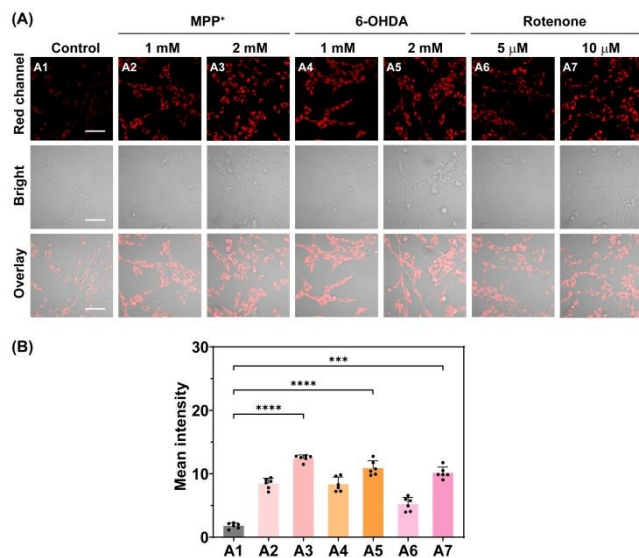


Fig. 4 (A) Fluorescence imaging of PD model cells following different pre-treatments and subsequent incubation with **DCI-HA-2** (10.0 μM) for 30.0 min: (A1) control; (A2) 1.00 mM MPP⁺ for 24 h; (A3) 2.00 mM MPP⁺ for 24 h; (A4) 1.00 mM 6-OHDA for 12 h; (A5) 2.00 mM 6-OHDA for 12 h; (A6) 5.00 μM rotenone for 1 h; (A7) 10.0 μM rotenone for 1 h. (B) Quantification of mean fluorescence intensity corresponding to panel (A). $\lambda_{\text{ex}} = 488 \text{ nm}$, $\lambda_{\text{em}} = 620\text{-}720 \text{ nm}$. Scale bar = 50.0 μm . Error bars represent SD, $n = 6$. **** $p < 0.0001$, *** $p < 0.001$.

conditions, PD cell models were established by exposing PC-12 cells to several neurotoxins, including 1-methyl-4-phenylpyridinium iodide (MPP⁺), 6-hydroxydopamine (6-OHDA), and rotenone, which are known to induce dopaminergic neuron loss.⁴² As shown in Fig. 4A, cells treated with each neurotoxin exhibited greatly enhanced red fluorescence compared with the control group, implying elevated intracellular HA levels in PD model cells. Quantitative analysis indicated that treatment with MPP⁺ (2.00 mM) resulted in a 6.92-fold increase in fluorescence intensity, while 6-OHDA (2.00 mM) and rotenone (10.0 μM) led to 5.95- and 5.63-fold increases, respectively (Fig. 4B). In addition, the elevation of HA was also observed in PD model SH-SY5Y cells and BV2 cells (Fig. S14). These findings convincingly demonstrate that HA is upregulated in PD model cells and further demonstrate that **DCI-HA-2** can reliably monitor intracellular HA fluctuations under PD-related pathological conditions.

Fluorescence imaging of HA variation in PD model mice

To investigate the intracerebral level of HA in PD conditions, PD model mice were established via intraperitoneal injection of 1-methyl-4-phenyl-1,2,3,6-tetrahydropyridine (MPTP) for 7 consecutive days. **DCI-HA-2** was then administered via tail vein injection to each group ($n = 6$ per group), and HA levels were evaluated by *in vivo* fluorescence imaging. As illustrated in Fig. 5A and S15, PD mice displayed markedly stronger fluorescence in the brain compared with the wild-type group, with intensity gradually increasing over time during blood circulation. After 12 h, the fluorescence intensity in the brains of PD mice was up to 2.05-fold compared with the control group (Fig. 5B). Then, brain tissues from each group were collected after euthanasia and subjected to imaging. As seen in Fig. S16, fluorescence imaging of brain tissue presented a 2.15-fold increase in PD mice compared with wild-type mice. In contrast, imaging of major

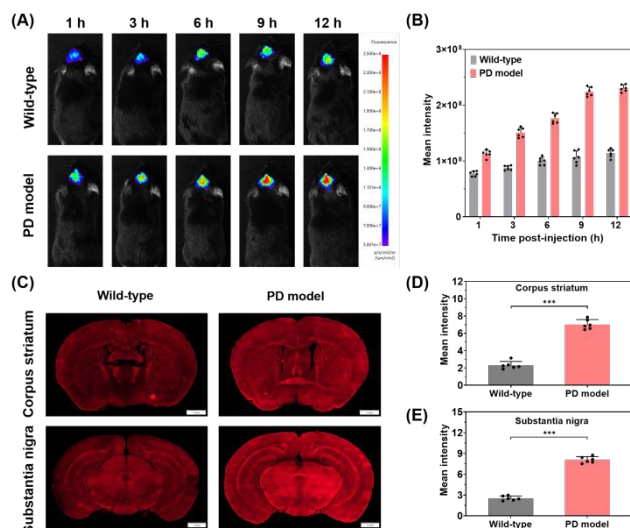


Fig. 5 (A) Fluorescence imaging of HA in wild-type and PD model mice after tail vein injection of **DCI-HA-2** (200 $\mu\text{g}/\text{kg}$). (B) Quantification of mean fluorescence intensity in panel (A). (C) Fluorescence imaging of HA in brain tissue slices of the corpus striatum and substantia nigra. (D, E) Quantification of mean red fluorescence intensity in the corpus striatum and substantia nigra. Red channel: **DCI-HA-2**, $\lambda_{\text{ex}} = 488 \text{ nm}$, $\lambda_{\text{em}} = 620\text{-}720 \text{ nm}$. Scale bar = 1.00 mm. Error bars represent SD, $n = 6$. *** $p < 0.001$.



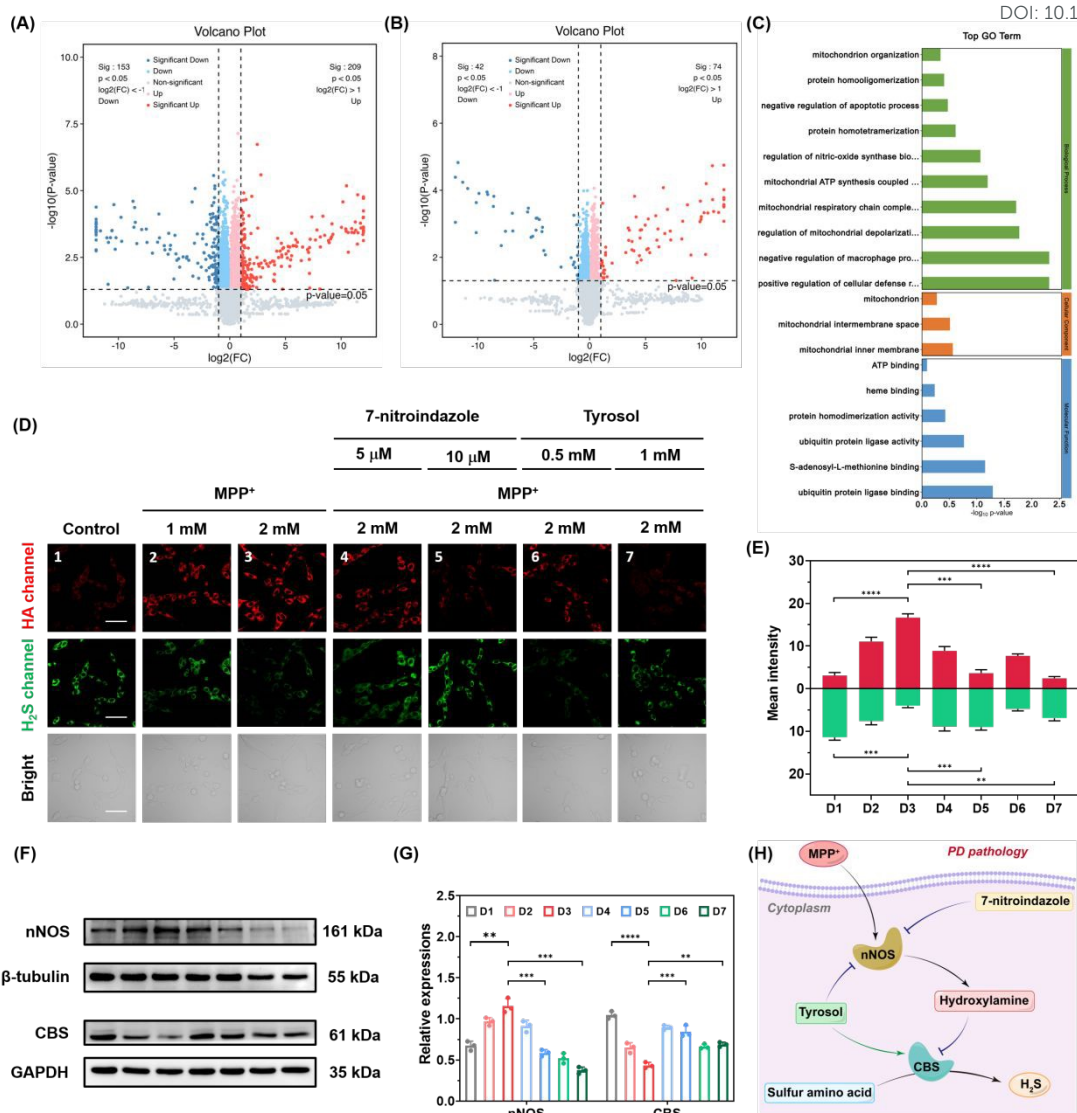


Fig. 6 Volcano maps of differentially expressed proteins for (A) PD group vs control group, and (B) 7-nitroindazole-treated PD group vs PD group. (C) GO enrichment analysis of differentially expressed proteins in the 7-nitroindazole treatment vs PD group. (D) Fluorescence images of PD model cells subjected to different pre-treatments before incubation with **DCI-HA-2** (10.0 μ M) and **N-H₂S** (10.0 μ M) for 30.0 min: (D1) control; (D2) 1.00 mM MPP⁺ for 24 h; (D3) 2.00 mM MPP⁺ for 24 h; (D4) 7-nitroindazole (10.0 μ M) for 8 h, followed by MPP⁺ (2.00 mM) for 24 h; (D5) 7-nitroindazole (20.0 μ M) for 8 h, followed by MPP⁺ (2.00 mM) for 24 h; (D6) tyrosol (0.50 mM) for 24 h, followed by MPP⁺ (2.00 mM) for 24 h; (D7) tyrosol (1.00 mM) for 24 h, followed by MPP⁺ (2.00 mM) for 24 h. (E) Quantification of mean fluorescence intensity in panel (D). (F) Western blots analysis of nNOS and CBS expression in cells from panel (D). (G) Semi-quantitative analysis of nNOS and CBS levels in (F). (H) Schematic illustration of HA-mediated regulation of cellular H₂S production in PD cells. Green channel, **N-H₂S**, $\lambda_{\text{ex}} = 405$ nm, $\lambda_{\text{em}} = 450$ –550 nm. Red channel, **DCI-HA-2**, $\lambda_{\text{ex}} = 488$ nm, $\lambda_{\text{em}} = 620$ –720 nm. Scale bar = 50.0 μ m. Error bars represent SD, $n = 3$. **** $p < 0.0001$, *** $p < 0.001$, ** $p < 0.01$.

organs showed minimal probe accumulation (Fig. S17), except in metabolic organs such as the liver and kidney, suggesting good BBB permeability and brain enrichment of **DCI-HA-2**. Additionally, the pharmacokinetic study of **DCI-HA-2** was investigated by collecting plasma and brain tissues. As seen in Fig. S18 and Table S2, the half-life time of **DCI-HA-2** was 5.34 h in the plasma and 9.44 h in the brain, suggesting relatively long systemic circulation time. Meanwhile, tissue distribution and clearance kinetics in liver and kidney were further evaluated. As depicted in Figs. S19 and S20, **DCI-HA-2** was mainly distributed in liver and kidney, with higher accumulation in liver than kidney. The clearance rates in liver and kidney were 1.11

mL/min and 3.68 mL/min, respectively, suggesting the renal excretion is the primary clearance pathway (Table S3). Given the pathological relevance of the corpus striatum and substantia nigra in PD,⁴³ brain slices were prepared and stained with DAPI for regional analysis. As shown in Figs. 5C–5E, brighter red fluorescence signals were significantly observed in these regions in PD mice than in the wild-type group, with 3.05- and 3.18-fold increases in the corpus striatum and substantia nigra, respectively. These results revealed that **DCI-HA-2** enables effective and specific visualization of elevated HA levels in the brains of PD mice.



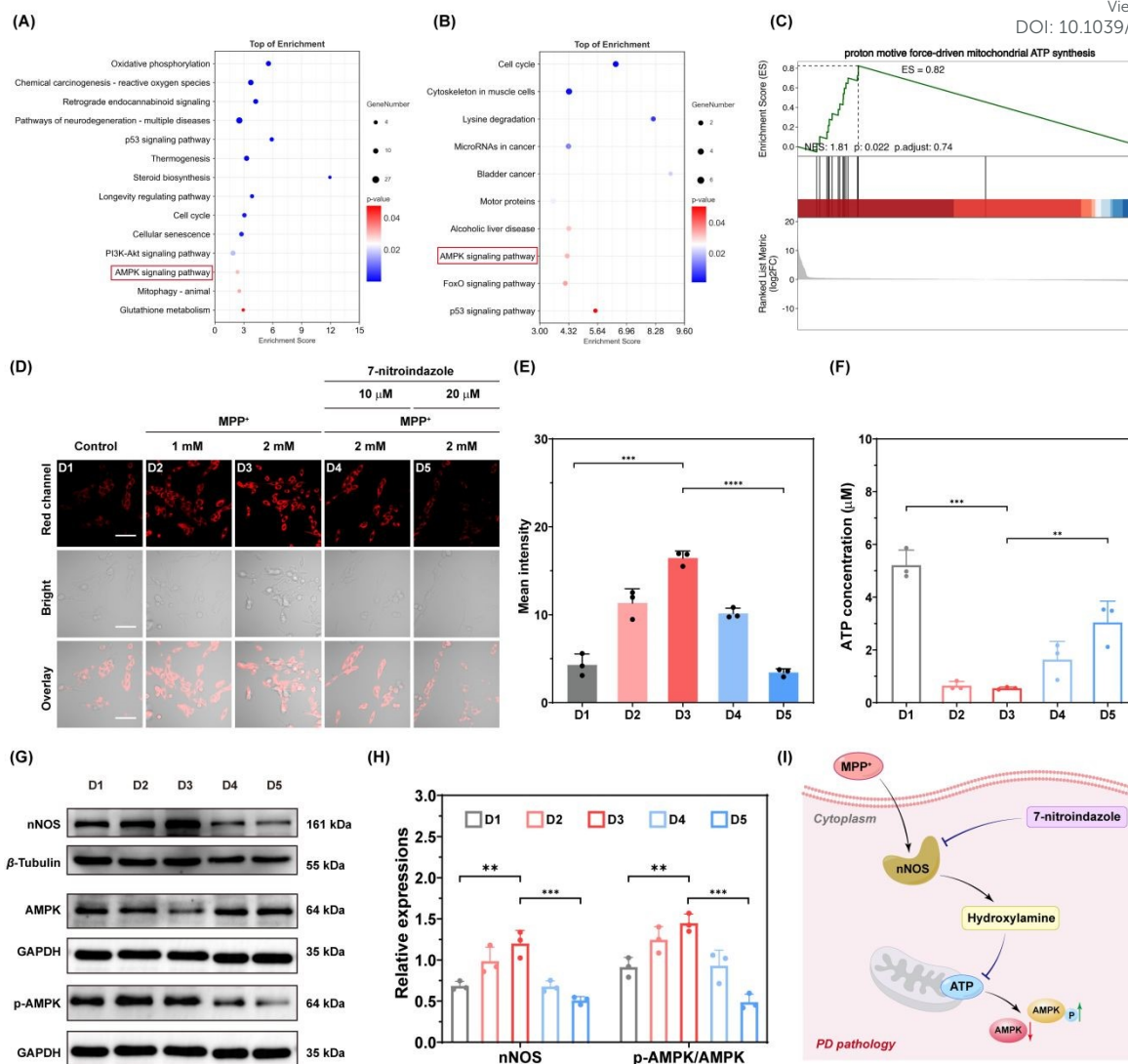


Fig. 7 KEGG pathway enrichment analysis of (A) PD group vs control group, and (B) 7-nitroindazole-treated PD group vs PD group cells. (C) Gene set enrichment analysis of ATP synthesis-related genes in 7-nitroindazole-treated PD group vs PD group cells. (D) Fluorescence images of PD model cells subjected to different pre-treatments before incubation with **DCI-HA-2** (10.0 μM) for 30 min: (D1) control; (D2) 1.00 mM MPP⁺ for 24 h; (D3) 2.00 mM MPP⁺ for 24 h; (D4) 7-nitroindazole (10.0 μM) for 8 h, followed by MPP⁺ (2.00 mM) for 24 h; (D5) 7-nitroindazole (20.0 μM) for 8 h, followed by MPP⁺ (2.00 mM) for 24 h. (E) Quantification of mean fluorescence intensity in panel (D). (F) Levels of ATP in panel (D). (G) Western blots analysis of nNOS, AMPK, and p-AMPK expression in cells from panel (D). (H) Semi-quantitative analysis of nNOS and p-AMPK/AMPK levels in panel (G). (I) Schematic illustration of HA-induced ATP depletion and downstream AMPK signaling dysfunction in PD cells. Red channel: **DCI-HA-2**, λ_{ex} = 488 nm, λ_{em} = 620–720 nm. Scale bar = 50.0 μm. Error bars represent SD, *n* = 3. **** *p* < 0.0001, *** *p* < 0.001, ** *p* < 0.01.

Regulatory role of HA in PD signaling pathways

To comprehensively clarify the regulatory involvement of HA in PD progression, proteomic analysis was performed on PC-12 cells from the control group, PD group (2.00 mM MPP⁺), and 7-nitroindazole-treated PD group (20.0 μM 7-nitroindazole followed by 2.00 mM MPP⁺) (Fig. S15). Proteomic analysis revealed various significantly differentially expressed proteins both in PD group vs control group (Fig. 6A) and 7-nitroindazole-treated PD group vs PD group (Fig. 6B). In addition, Gene Ontology (GO) functional enrichment analysis of proteins in PD group altered by 7-nitroindazole treatment (Fig. 6C and S16) indicated strong associations with mitochondrial respiration and several CBS-related functional categories, including S-adenosyl-L-methionine binding, ubiquitin protein ligase

binding, heme binding and protein homodimerization. These findings hinted that HA metabolism may be closely linked to the regulation of CBS activity and its function. Given that CBS activity governs H₂S biosynthesis,⁴⁴ and that HA is overexpressed in PD models, these results raise the intriguing possibility that endogenous HA may participate in the regulation of H₂S production during PD progression.

To address this question, we investigated the connection between HA and H₂S in MPP⁺-induced PD model cells using the HA probe **DCI-HA-2** and a H₂S fluorescent probe **N-H₂S** (Scheme S4). As depicted in Fig. 6D, MPP⁺-treated PD model cells displayed stronger HA-associated red fluorescence and weaker H₂S-associated green fluorescence than control group. Notably, the increase in red fluorescence and the decrease in green



fluorescence became more pronounced with increasing MPP⁺ concentration. In particular, PD cells induced by MPP⁺ (2.00 mM) showed a 5.41-fold increase in red fluorescence and a 0.35-fold decrease in green fluorescence, suggesting HA overexpression accompanied by reduced H₂S levels in PD cells. To prove the cascade relationship between HA and H₂S, cells were successively pre-treated with 7-nitroindazole (20.0 μM) and MPP⁺ (2.00 mM), followed by staining with **DCI-HA-2** and **N-H₂S**. Under these conditions, the red fluorescence decreased to 0.22-fold, while the green fluorescence increased to 2.19-fold compared with MPP⁺(2.00 mM)-incubated cells, suggesting that inhibition of HA generation leads to recovery of intracellular H₂S levels. In addition, tyrosol, a known CBS activator, was used to upregulate the activity of CBS.⁴⁵ Cells pre-treated with tyrosol (1.00 mM) prior to MPP⁺ (2.00 mM) exposure showed a 1.72-fold increase in H₂S-related green fluorescence and a 0.15-fold decrease in HA-related red fluorescence (Fig. 6E), implying that tyrosol promotes H₂S production while reducing cellular HA levels. To fully understand the above phenomenon, western blot (WB) analysis was performed to analyse the expression of nNOS and CBS under the above conditions (Figs. S18 and S19). As illustrated in Figs. 6F and 6G, compared with the control group, cells treated with 2.00 mM MPP⁺ showed upregulated expression of nNOS (1.71-fold) and downregulated expression of CBS (0.42-fold), which was consistent with the imaging results. Moreover, pre-treatment with 7-nitroindazole (20.0 μM) decreased the nNOS level to 0.49-fold and enhanced CBS level to 1.90-fold in comparison with MPP⁺ (2.00 mM)-treated group, demonstrating a negative correlation between HA production and CBS expression. Similarly, cells pre-treated with tyrosol (1.0 mM) followed by MPP⁺ (2.00 mM) resulted in a 1.51-fold elevation in CBS level. Notably, a pronounced decrease in nNOS expression (0.34-fold) was also observed, likely due to the inhibitory effect of tyrosol on nNOS activity,⁴⁶ which also explains the reduced HA-related red fluorescence observed in Fig. 5D. Taken together, these results reveal, for the first time, that elevated levels of HA derived from nNOS inhibits the expression of CBS, thereby diminishing the production of H₂S in PD pathological cells (Fig. 6H).

Next, we additionally delved into the regulatory role of HA in PD cells. Kyoto Encyclopedia of Genes and Genomes (KEGG) pathway enrichment analysis revealed two biological pathways in both PD group vs control group (Fig. 7A) and 7-nitroindazole-treated PD group vs PD group (Fig. 7B), namely p53 signaling pathway and the AMPK signaling pathway. In particular, gene set enrichment analysis also showed that 7-nitroindazole treatment markedly upregulated genes associated with ATP synthesis in PD cells (Figs. 7C and S17), prompting us to investigate the involvement of HA in cellular energy metabolism. Similar to the above, an elevated level of HA was detected in PD cells (Fig. 7D), and the pre-treated with 7-nitroindazole can significantly inhibit the generation of cellular HA in PD cells (Fig. 7E). To determine whether the alteration of HA is associated with ATP synthesis-related signaling pathway in PD, a commercial ATP assay kit was employed to quantify the intracellular ATP contents under above conditions. It was seen that the level of ATP in 2.00 mM MPP⁺-treated cells was markedly reduced to 0.55 μM, corresponding to an 89.44% decrease compared with the control group (5.21 μM), revealing pronounced ATP depletion under PD conditions (Fig. 7F). In contrast, pre-treatment with 7-nitroindazole (20.0 μM) led to a 5.63-fold recovery of ATP levels (3.04 μM) relative to MPP⁺

treatment alone, indicating that suppression of HA production effectively promotes ATP synthesis. To further assess the involvement of HA in ATP-related AMPK signaling, WB analysis was performed to examine the expression of nNOS, AMPK and phosphorylated-AMPK (p-AMPK) under different treatment conditions (Figs. S20-S22). As shown in Figs. 7G and 7H, nNOS expression was increased by 1.75-folds in 2.00 mM MPP⁺ treatment relative to control cells, consistent with the elevated HA level (brighter red fluorescence), whereas 7-nitroindazole (20.0 μM) treatment reduced nNOS expression by 57.6%. Moreover, the p-AMPK/AMPK ratio increased by 1.32-fold following 2.00 mM MPP⁺ treatment, implying the dysregulated AMPK signalling in PD. Notably, pre-treatment with 7-nitroindazole (20.0 μM) decreased the p-AMPK/AMPK ratio by 66.2% relative to 2.00 mM MPP⁺ treatment alone, suggesting that the inhibition of HA generation ameliorates ATP synthesis and normalizes AMPK signaling. Overall, these results demonstrate that nNOS-derived HA inhibits ATP synthesis and disrupts AMPK signaling pathway during PD pathology, highlighting HA as a critical metabolic regulator in PD progression (Fig. 7I).

Conclusions

In conclusion, we have established a universal strategy for constructing highly specific HA-activated fluorescent probes across various fluorescent scaffolds based on chemo-selective cleavage and intramolecular nucleophilic cascade reactions, enabling sensitive and selective detection of HA in complex biological environments. The optimized probe, **DCI-HA-2**, enabled, for the first time, the real-time visualization of HA overexpression in PD cells and PD model mice. By integrating fluorescence imaging with comprehensive proteomic analysis, we revealed that nNOS-derived HA suppresses CBS, impairing H₂S biosynthesis, and simultaneously induces ATP depletion, thereby disrupting AMPK signaling in PD pathology. These results establish HA as a previously unrecognized pathological mediator and highlight **DCI-HA-2** as a versatile tool for probing HA-associated signaling in complex biological systems. This work offers new mechanistic insights into PD progression and lays a foundation for future diagnostic and therapeutic strategies targeting HA-mediated pathways.

Ethical statement

All animal experiments were carried out in accordance with national guidelines and all procedures were approved by the ethical committees of Central South University (No. 430727211101478756) and Zhejiang University (ZJU20250124).

Author contributions

S. Z. and J. K. contributed equally to this work. S. Z. and X. S. conceived the ideas and designed the studies. S. Z. and H. Z. carried out the synthesis and photophysical studies. S. Z. and J. K. performed the *in vivo* imaging and proteins studies. S. Z., B. W. and X. S. wrote the manuscript. B. W., C. Y., M. L. and X. S. guided the process. All authors reviewed and approved the final version of the manuscript.



Conflicts of interest

There are no conflicts to declare.

Data availability

The data of this study are available in the ESI†.

Acknowledgements

This work was supported by the National Natural Science Foundation of China (Nos. 22278447 and 22178395) and Natural Science Foundation of Hunan Province (Nos. 2024JJ4050 and 2023JJ40793).

Notes and references

1. Y. Ben-Shlomo, S. Darweesh, J. Llibre-Guerra, C. Marras, M. San Luciano and C. Tanner, *The Lancet*, 2024, **403**, 283-292.
2. W. Poewe, K. Seppi, C. M. Tanner, G. M. Halliday, P. Brundin, J. Volkman, A.-E. Schrag and A. E. Lang, *Nat. Rev. Dis. Primers*, 2017, **3**, 17013.
3. H. R. Morris, M. G. Spillantini, C. M. Sue and C. H. Williams-Gray, *The Lancet*, 2024, **403**, 293-304.
4. M. J. Armstrong and M. S. Okun, *JAMA*, 2020, **323**, 548-560.
5. S. Przedborski and H. Ischiropoulos, *Antioxid. Redox Sign.*, 2005, **7**, 685-693.
6. S. Z. Imam, G. D. Newport, Y. Itzhak, J. L. Cadet, F. Islam, W. Slikker Jr and S. F. Ali, *J. Neurochem.*, 2001, **76**, 745-749.
7. J. L. O'Connor, D. M. Fountos, B. Firouzan, F. Azizi, R. Ghasemi and K. Kashfi, *Neurotherapeutics*, 2025, **22**, e00710.
8. A. J. Väänänen, M. Moed, R. K. Tuominen, T. H. Helkamaa, M. Wiksten, P. Liesi, C. C. Chiueh and P. Rauhala, *Free Radical Res.*, 2003, **37**, 381-389.
9. H. C. Çubukçu, M. Yurtdaş, Z. E. Durak, B. Aytaç, H. N. Güneş, B. G. Çokal, T. K. Yoldaş and İ. Durak, *Neurol. Sci.*, 2016, **37**, 1793-1798.
10. Y. Kono and I. Fridovich, *J. Biol. Chem.*, 1983, **258**, 13646-13648.
11. P. Gross and R. P. Smith, *CRC Crit. Rev. Toxicol.*, 1985, **14**, 87-99.
12. N. Aleksidze and C. Blomstrand, *Brain Res.*, 1968, **11**, 717-719.
13. N. A. Correia, R. B. Oliveira and G. Ballejo, *Life Sci.*, 2000, **68**, 709-717.
14. H. Zhu, Z. Ma, X. Wang, L. Ji and B. Zhu, *Coord. Chem. Rev.*, 2025, **544**, 216963.
15. S. Wang, H. Song, C. Yin and F. Huo, *Coord. Chem. Rev.*, 2025, **543**, 216940.
16. L. Gao, W. Wang, X. Wang, F. Yang, L. Xie, J. Shen, M. A. Brimble, Q. Xiao and S. Q. Yao, *Chem. Soc. Rev.*, 2021, **50**, 1219-1250.
17. J. Zhou, P. Jangili, S. Son, M. S. Ji, M. Won and J. S. Kim, *Adv. Mater.*, 2020, **32**, 2001945.
18. J. Wang, M. Cao, L. Han, P. Shangguan, Y. Liu, Y. Zhong, C. Chen, G. Wang, X. Chen, M. Lin, M. Lu, Z. Luo, M. He, H. H. Y. Sung, G. Niu, J. W. Y. Lam, B. Shi and B. Z. Tang, *J. Am. Chem. Soc.*, 2024, **146**, 28783-28794.
19. H. Li, J. Wang, H. Kim, X. Peng and J. Yoon, *Angew. Chem. Int. Ed.*, 2024, **63**, e202311764.
20. A. C. Sedgwick, R. S. L. Chapman, J. E. Gardiner, L. R. Peacock, G. Kim, J. Yoon, S. D. Bull and T. D. James, *Chem. Commun.*, 2017, **53**, 10441-10443.
21. B. Dong, M. Tian, X. Kong, W. Song, Y. Lu and W. Lin, *Anal. Chem.*, 2019, **91**, 11397-11402. DOI: 10.1039/D6SC01655C
22. P. Rana, L. Panda, N. Murmu, B. P. Bag and S. N. Sahu, *Org. Biomol. Chem.*, 2020, **18**, 5963-5971.
23. W. Du, Y. Tian, Y.-A. Feng, X.-W. Cong, R. Tan, Y.-W. Wang and Y. Peng, *Anal. Chim. Acta*, 2024, **1318**, 342941.
24. M. Du, H. Jiang, M. Song, Y. Zhang, H. Lv, S. Zhao, H. Du and Z. Dong, *Anal. Methods*, 2024, **16**, 4843-4855.
25. J. Ma, M. Zhao, X. Kong, Y. Liu, D. Meng and Z. Zhang, *Dyes Pigm.*, 2026, **245**, 113218.
26. A. C. Sedgwick, R. S. L. Chapman, J. E. Gardiner, L. R. Peacock, G. Kim, J. Yoon, S. D. Bull and T. D. James, *Chem. Commun.*, 2017, **53**, 10441-10443.
27. Z. Liu, X. Zhou, Y. Miao, Y. Hu, N. Kwon, X. Wu and J. Yoon, *Angew. Chem. Int. Ed.*, 2017, **56**, 5812-5816.
28. Y. Yue, F. Huo, P. Ning, Y. Zhang, J. Chao, X. Meng and C. Yin, *J. Am. Chem. Soc.*, 2017, **139**, 3181-3185.
29. D. Cheng, Y. Pan, L. Wang, Z. Zeng, L. Yuan, X. Zhang and Y.-T. Chang, *J. Am. Chem. Soc.*, 2017, **139**, 285-292.
30. A. C. Sedgwick, R. S. L. Chapman, J. E. Gardiner, L. R. Peacock, G. Kim, J. Yoon, S. D. Bull and T. D. James, *Chem. Commun.*, 2017, **53**, 10441-10443.
31. D. Cheng, Y. Pan, L. Wang, Z. Zeng, L. Yuan, X. Zhang and Y.-T. Chang, *J. Am. Chem. Soc.*, 2017, **139**, 285-292.
32. J. J. Díaz-Mochón, L. Bialy and M. Bradley, *Org. Lett.*, 2004, **6**, 1127-1129.
33. J. Andersonmckay, G. P. Savage and G. W. Simpson, *Aust. J. Chem.*, 1996, **49**, 163-166.
34. E. Suárez-Picado, S. K. Ahirwar and L. R. Malins, *Org. Lett.*, 2026, **28**, 1815-1820.
35. W. Zhang, F. Huo and C. Yin, *J. Mater. Chem. B*, 2018, **6**, 6919-6929.
36. L. Dai, Q. Zhang, Q. Ma and W. Lin, *Coord. Chem. Rev.*, 2023, **489**, 215193.
37. F. Liu, X. Ding, X. Xu, F. Wang, X. Chu and J.-H. Jiang, *Angew. Chem. Int. Ed.*, 2022, **61**, e202203243.
38. A. Alouane, R. Labruère, T. Le Saux, F. Schmidt and L. Jullien, *Angew. Chem. Int. Ed.*, 2015, **54**, 7492-7509.
39. W. Wei, C. Huang, J. Zhang, Q. Chen, Z. Liu, X. Ren, S. Gan, P. Wu, D. Wang, B. Z. Tang and H. Sun, *Anal. Chem.*, 2024, **96**, 2406-2414.
40. T. L. Poulos and H. Li, *Acc. Chem. Res.*, 2013, **46**, 390-398.
41. P. E. Erik, A. L. Elizabeth, S. Jiwon, Z. Yaoqiu, J. Haitao and B. S. Richard, *Curr. Top. Med. Chem.*, 2005, **5**, 603-624.
42. D. Blum, S. Torch, N. Lambeng, M.-F. Nissou, A.-L. Benabid, R. Sadoul and J.-M. Verna, *Prog. Neurobiol.*, 2001, **65**, 135-172.
43. Y. Lu, X. Zhang, L. Zhao, C. Yang, L. Pan, C. Li, K. Liu, G. Bai, H. Gao and Z. Yan, *Front. Neurosci.*, 2018, **12**, 2018.
44. Y.-W. Wang, T. Chu, X.-L. Wang, Y.-Q. Fan, L. Cao, Y.-H. Chen, Y.-W. Zhu, H.-X. Liu, X.-Y. Ji and D.-D. Wu, *Cell. Signal.*, 2024, **124**, 111406.
45. L. K. Sarna, V. Sid, P. Wang, Y. L. Siow, J. D. House and K. O., *Lipids*, 2016, **51**, 583-590.
46. P. Dewapriya, S. W. A. Himaya, Y.-X. Li and S.-K. Kim, *Food Chem.*, 2013, **141**, 1147-1157.



The data of this study are available in the ESI†.

View Article Online
DOI: 10.1039/D6SC01655C

